NASA MEMO 4-27-59A

NASA

MEMORANDUM

LIFT-DRAG RATIOS FOR AN ARROW WING WITH BODIES AT MACH NUMBER 3

By Leland H. Jorgensen

Ames Research Center
Moffett Field, Calif.

NATIONAL AERONAUTICS AND SPACE ADMINISTRATION

May 1959
Declassified May 29, 1961

NATIONAL AERONAUTICS AND SPACE ADMINISTRATION

MEMORANDUM 4-27-59A

LIFT-DRAG RATIOS FOR AN ARROW WING WITH BODIES AT MACH NUMBER 3*

By Leland H. Jorgensen

SUMMARY

Force and moment characteristics, including lift-drag ratios, have been measured for bodies of circular and elliptic cross section alone and combined with a warped arrow wing. The test Mach number was 2.94, and the Reynolds number was 3.5×10^6 (based on wing mean aerodynamic chord). The experimental results show that for equal volume the use of an elliptical body can result in a noticeably higher maximum lift-drag ratio than that obtained through use of a circular body.

Methods for estimating the aerodynamic characteristics have been assessed by comparing computed with experimental results. Because of good agreement of the predictions with experiment, maximum lift-drag ratios have been computed for the arrow wing in combination with bodies of various sizes. These calculations have shown that, for an efficient wing-body combination, little loss in maximum lift-drag ratio results from considerable extension of afterbody length. For example, for a wing-body configuration having a maximum lift-drag ratio of about 7.1, a loss in maximum lift-drag ratio of less than 0.2 results from a 40-percent increase in body volume by extension of afterbody length. It also appears that with body length fixed, maximum lift-drag ratio decreases almost linearly with increase in body diameter. For a wing-body combination employing a body of circular cross section, a decrease in maximum lift-drag ratio from about 9.1 for zero body diameter to about 4.6 for a body diameter of 13.5 percent of the body length was computed.

INTRODUCTION

It is well known that the range of an aircraft in relatively steady level flight depends on the ratio of lift to drag. From the range equation it is also known that the range is proportional to the thermopropulsive

*Title, Unclassified

efficiency and the logarithm of the ratio of initial to final weight. Obviously, some unorthodox aircraft designs based entirely upon considerations for achieving a high lift-drag ratio may not be practical at the present time because of weight and structural limitations. Nevertheless, the aerodynamicist has the obligation to point out the directions in which to proceed for greater aerodynamic efficiency. In reference 1 by Brown and McLean and in reference 2 by R. T. Jones some theoretical possibilities for obtaining high lift-drag ratios are reviewed. From these studies it is evident that arrow or sweptback wings offer considerable hope for obtaining high lift-drag ratios at supersonic speeds. Katzen, in reference 3, also reaches this conclusion in studying the lift-drag ratios that are theoretically possible to achieve with delta and arrow wings at Mach number 3. In tests reported in reference 3 of an arrow wing designed for high lift-drag ratio at Mach number 3, an experimental trimmed lift-drag ratio of about 9 was obtained. This value, although lower than the estimated result of about 11.5, is probably the highest measured for a model at Mach number 3 with an essentially turbulent boundary layer.

Of considerable interest, of course, is the effect on lift-drag ratio of adding body volume to an efficient wing. In the present investigation such a study has been undertaken. The arrow wing of reference 3 has been tested in combination with both a body of circular cross section and a body of elliptic cross section. In addition, measured values of lift and drag coefficient for the wing alone have been used to compute lift-drag ratios for the wing in combination with bodies of various sizes. The purpose of this report is twofold: first, to assess the adequacy of a proposed method for computing the aerodynamic characteristics of an arrow wing-body combination by comparing computed with experimental results and, second, to show the predicted magnitudes of the maximum lift-drag ratios resulting from the addition of various amounts of body volume to an efficient arrow wing.

NOTATION

A_b body base area

A_p body plan-form area

A_W exposed wing plan-form area

a semimajor axis of elliptic cross section

b semiminor axis of elliptic cross section

C_{d_c} section drag coefficient of circular cylinder, based on cylinder diameter

C_D drag coefficient, $\frac{D}{q_\infty A_W}$

C_{D_o} drag coefficient at zero lift

C_L lift coefficient, $\frac{L}{q_\infty A_W}$

C_m pitching-moment coefficient at specified length position x_m, $\frac{\text{pitching moment}}{q_\infty A_W \bar{c}}$

c wing root chord

$\bar{c}$ wing mean aerodynamic chord

D drag (exclusive of body base drag)

d body base diameter, $2\sqrt{ab}$ for an elliptic body

K ratio of lift component to lift of wing alone

L lift

l body length

$\bar{l}$ distance to center of pressure measured from intersection of wing leading edge and body

l_N body nose length

M_∞ free-stream Mach number

Q body volume

q_∞ free-stream dynamic pressure

R Reynolds number based on wing mean aerodynamic chord

r local body radius

x,y,z Cartesian coordinates with origin at body nose vertex, x axis coincident with body longitudinal axis, and z axis perpendicular to x axis in pitch plane

$\bar{x}$ distance from nose vertex to center-of-pressure position

x_c distance from nose vertex to centroid of body plan-form area

x_{le} distance from wing apex to wing leading edge (see fig. 1)

x_m distance from nose vertex to pitching-moment reference center

x_o wing ordinate measured along chord from wing leading edge (see fig. 1)

α angle of attack

β $\sqrt{M_\infty^2-1}$

ϵ semiapex angle of wing leading edge

φ angle of bank about body longitudinal axis

Subscripts

B body

B(W) body in presence of wing

e elliptic cross section

i interference

L lower surface of wing

max maximum

U upper surface of wing

W wing

W(B) wing in presence of body

APPARATUS AND TESTS

Wind Tunnel

The experimental investigation was conducted in the Ames 1- by 3-foot supersonic wind tunnel No. 2. This tunnel is a nonreturn, intermittent-operation type and is equipped with a flexible-plate nozzle that provides

a variation of Mach number from 1.4 to 3.8. Air for this tunnel is obtained from the Ames 12-foot pressure wind tunnel at a pressure of about 5 atmospheres and is expanded through the nozzle to the atmosphere. Changes in Reynolds number are obtained by varying the total pressure. The water content of the air is maintained at less than 0.0003 pound of water per pound of dry air. Consequently, the effect of humidity on the flow is negligible.

Models

Plan-form views of the models tested are shown in figure 1. The arrow wing (W) of figure 1(a) is model 6 of reference 3. This wing was designed for $\beta \tan \epsilon = 0.5$ at $M_\infty = 3$ and was cambered and twisted for low drag due to lift. Previous to being twisted, the wing section normal to the leading edge was the Clark Y, 12 percent thick. Several of the wing sections for the twisted wing are shown in the lower half of figure 1(a). It is seen that the wing tips are bent upward, the bend starting at the trailing edge of the root section. Ordinates for the bent wing are tabulated in table I. Because it gave the highest trimmed lift-drag ratio (about 9) of any of the arrow wings previously tested (ref. 3) at Mach number 3, this wing was chosen for additional tests with the bodies shown in figures 1(b) and 1(c). Body B_1, shown in figure 1(b) with wing W, had a circular cross section and consisted of a nose of fineness ratio 6 [$r = (d/2)(x/l_N)^{3/4}$] with a cylindrical afterbody 10 diameters long. Body B_2, shown in figure 1(c) with wing W, had an elliptic cross section ($a/b = 2$), and the axial distribution of cross-sectional area was the same as for body B_1. Hence, the fineness ratio of $l/d = 16$ for B_1 was also the equivalent fineness ratio for B_2.

The wing (W) and the bodies (B_1 and B_2) were interchangeable and could be tested alone or in combination. The wing was positioned on the bodies so that the bottom surface at the root chord was essentially at the midbody position $z = 0$, and the entire cambered top surface was above the midbody position. Actually the z wing ordinates in table I are taken with respect to the body z axis and, hence, give the position of the wing with respect to the bodies. All of the models were constructed of steel and were supported from the rear on a strain-gage balance.

Tests

Force tests.- Balance measurements of lift, drag, and pitching moment were obtained for bodies B_1 and B_2 alone and combined with wing W (models B_1W and B_2W) at a free-stream Mach number of 2.94. The Reynolds

number, based on wing mean aerodynamic chord, was 3.5×10^6. The angle-of-attack range was from about 0° to 13° for bodies B_1 and B_2. For models B_1W and B_2W the angle-of-attack range was from about -6.5° to $+6.5^\circ$. The arrow wing W has been previously tested alone at the same Mach number and Reynolds number and for angles of attack from -6.5° to $+6.5^\circ$ (ref. 3). For the bodies and wing-body combinations, base pressures from eight orifices spaced around the inside of the base periphery of each model were measured from photographic recordings of a multiple-tube manometer board.

Visual-flow tests.- The sublimation technique (ref. 4) was used for determining the position of boundary-layer transition on the models. The models, which were initially painted black, were sprayed with a saturated solution of tetrachlorobenzene in benzene. This solution dries on contact with the model surface and presents a white appearance. As the wind tunnel is operated, the process of sublimation takes place with turbulent boundary-layer regions showing up as dark areas on the model and laminar regions remaining white. (Other solutions, such as biphenyl, acenaphthene, or azobenzene dissolved in petroleum ether, can be used to produce progressively slower rates of sublimation for tests in longer running wind tunnels of the closed-circuit continuous-operation type.)

In addition to the sublimation technique, flow patterns were visualized through use of the white-lead (liquid film) method (ref. 5). In this technique the models are painted with a mixture of white lead and light lubricating oil (S.A.E. 10) and are run wet in the wind tunnel. Flow directions and regions of separation become discernible on the surface.

REDUCTION AND ACCURACY OF DATA

All of the force and moment data have been reduced to coefficient form. The average base pressure from the eight base orifices was used to compute the base drag which was subtracted from the total axial-force balance measurement, so that the data presented are for forces ahead of the body base. Actually there was little difference in the base pressures from the eight base orifices, and fewer orifices could have been used.

The accuracy of the final data is affected by uncertainties in the measurement of the forces and moments, and in the determination of the stream static and dynamic pressures used in reducing the forces and moments to coefficient form. These individual uncertainties led to estimated uncertainties which are listed below.

C_L	± 0.002	L/D	± 0.1
C_D	$\pm .0002$	$\bar{x}/l$	$\pm .02$
C_m	$\pm .002$		

The values of angle of attack are estimated to be accurate to within $\pm 0.1^{\circ}$. The variation of the free-stream Mach number in the region of the test models was less than ±0.02 at Mach number 2.94.

RESULTS AND DISCUSSION

Experimental Results

Experimental results of lift, drag, lift-drag ratio, pitching moment, and center of pressure are plotted in figure 2 for all of the models tested. Sketches of the models in plan-form view are used to identify the curves, a practice followed throughout the report. It is seen in figure 2(a) that the elliptic body B_2 develops about twice the lift of the circular body B_1. As a result, the lift coefficients based on the exposed wing area are also higher for the wing-body combination employing the elliptic body (B_2W) than for the combination with the circular body (B_1W). The wing-body combination having the elliptic body (B_2W) also develops higher lift-drag ratios, $(L/D)_{max}$ being about 7.2 for B_2W as compared to 6.7 for B_1W (see fig. 2(c)). For the pitching-moment results presented in figure 2(d), the moment reference positions, x_m, are chosen so that the wing and wing-body combinations are trimmed at the lift coefficients for $(L/D)_{max}$. The wing-body combinations were found to be longitudinally stable about these positions. The moment data for the bodies alone are referred to the same positions as for the corresponding wing-body combinations. As shown in figure 2(e), the center-of-pressure positions are slightly more forward for the models with elliptic bodies than for the corresponding models with circular bodies. As a result, the moment reference position for B_2W (at $x_m = 0.690\ l$) is slightly forward of that for B_1W (at $x_m = 0.715\ l$).

From sublimation tests it was observed that the boundary-layer flow over the models was mostly turbulent. In figure 3 photographs are shown of patterns resulting from a sublimation test of model B_2W at $\alpha = 0^{\circ}$. It can be seen that laminar flow regions, which are white, are found only near the body vertex and the wing leading edges. With increase in angle of attack to about 6.5° (the highest of this investigation for B_2W), the small length of laminar run on the model appeared to diminish. (Note that in the photographs presented in this report a small amount of wing near the tips is removed. It was found, however, that this loss of tip had negligible effect on the flow patterns obtained by both the sublimation and white-lead techniques.)

In figure 4 photographs are shown of secondary flow patterns resulting from white-lead tests of model B_2W at $\alpha = 0^\circ$ and $\alpha = 4.5^\circ$. At $\alpha = 0^\circ$ (fig. 4(a)) the patterns indicate that the flow was attached over the top surface of the model. Over the bottom, however, there is evidence of some flow separation from the wing rearward of the position at which the bending up of the wing was started. At $\alpha = 4.5^\circ$, the angle for $(L/D)_{max}$, the patterns in figure 4(b) indicate that the flow was attached over the bottom surface, but on the top there was some separation near the wing leading edges (as indicated by the ridge lines near and parallel to the leading edges).

Comparisons of Predicted and Experimental Results

Predicted and experimental aerodynamic characteristics for the bodies and wing-body combinations tested are compared in figures 5 and 6. The circular body B_1 and wing-body combination B_1W are considered in figure 5, and the elliptic body B_2 and wing-body combination B_2W are considered in figure 6. The experimental wing alone results are presented in both figures for reference, since they were used in computing the aerodynamic characteristics of the wing-body combinations. In general, the computed curves, which were determined by the methods outlined in the appendix, are in good agreement with the experimental results. It should be noted, however, that the prediction of lift coefficient as a function of angle of attack is slightly erroneous (figs. 5(a) and 6(a)). This disagreement probably results from omission in the calculation of the interference lift caused by placement of the wing above the midbody $z = 0$ location. With the cambered upper surface of the wing entirely above the midbody location (the bottom surface near the root chord being essentially at $z = 0$), a positive pressure field was probably created over part of the body top, resulting in some negative interference lift. The magnitude of the interference lift coefficient at $\alpha = 0^\circ$ can be seen in figures 5(a) and 6(a). Here the negative lift coefficient at $\alpha = 0^\circ$ can be attributed mostly to interference, since the body-alone lift coefficient is zero, and the wing-alone lift coefficient is practically zero.

The agreement of the computed with the experimental center-of-pressure positions in figures 5(e) and 6(e) is surprisingly good considering the assumptions in the theoretical methods. For the wing-body combinations the computed center-of-pressure positions are generally slightly forward of the experimental positions. As a result, the computed and experimental pitching-moment coefficients are somewhat in disagreement (see figs. 5(d) and 6(d)).

Effect of Body Size on Maximum Lift-Drag Ratio

Because of the satisfactory agreement of calculated with experimental values of $(L/D)_{max}$ for the models tested, additional calculations of $(L/D)_{max}$ have been made for wing-body combinations employing bodies of various sizes. The body size was mainly varied by changing the body diameter with the length fixed. However, with the body diameter kept constant at the value for the test model B_1W ($d = 0.936$ inch or $0.062\ l$), the effect on $(L/D)_{max}$ of extending the afterbody length to the wing tips was computed. This extension of afterbody length increased the total body length from about 16 to 21 diameters, and the body volume increased about 40 percent. With this large increase in body length and volume, however, the computed loss in $(L/D)_{max}$ was less than 0.2. A similar result is reported in reference 6 for flat-top arrow-wing configurations with half cones mounted below thin wings. Here it is shown from experiment that a 40-percent increase in body volume, by increase in afterbody length, results in practically no loss in measured lift-drag ratio.

With the body length kept constant at the same value as for the test models B_1W and B_2W, the variation of $(L/D)_{max}$ with change in body diameter was computed for values of d from 0 to $0.135\ l$. The computed results are presented in figure 7. Experimental values of $(L/D)_{max}$ for the wing W alone and for the wing-body combinations, B_1W and B_2W, are also shown for comparison. It is seen that, for wing-body combinations employing bodies of circular cross section, there is a steady decrease in $(L/D)_{max}$ from about 9.1 for $d = 0$ to about 4.6 for $d = 0.135\ l$. Loss in $(L/D)_{max}$ with increase in d/l is apparently diminished somewhat through use of a body of elliptic cross section.

In figure 8 the results of figure 7 are replotted with the abscissa changed to $\frac{(\text{body volume})^{2/3}}{\text{total plan area}}$. Here the calculation shows that for large equal values of this parameter the configurations with the circular bodies should be slightly more efficient than the ones with the elliptic bodies. This, of course, is because of the fact that wing area is more efficient than body area, and a greater percentage of the total plan area is wing area for the configurations with the circular bodies than for those with elliptic bodies. Also plotted in figure 8 is the value of $(L/D)_{max}$ of 7.4 reported in reference 3 for the arrow wing in combination with a circular body of smaller diameter (0.75 inch) than the one used for the tests of this investigation. As shown in figure 8, the agreement of the computed with the experimental results is good.

If it is assumed that wing volume is essentially useful volume, $(L/D)_{max}$ can be plotted as a function of the total volume parameter, $\frac{(\text{total volume})^{2/3}}{\text{total plan area}}$. The computed and experimental values of $(L/D)_{max}$

are plotted as a function of this parameter in figure 9. It is seen that there is a rapid decrease in $(L/D)_{max}$ resulting from addition of body volume to wing volume. This illustrates the great loss in aerodynamic efficiency which results from the use of bodies for increasing volume capacity. The indication is, of course, that for greatest aerodynamic efficiency, volume should be designed into the wing.

CONCLUSIONS

An efficient arrow wing combined with bodies of circular and elliptic cross section has been tested at Mach number 2.94. The Reynolds number, based on wing mean aerodynamic chord, was 3.5×10^6. Bodies of circular and elliptic cross section also have been tested alone at the same conditions. Computed values of lift, drag, lift-drag ratio, pitching moment, and center of pressure have been compared with measured values. An analysis of the results has led to the following conclusions:

1. The experimental results show that for equal volume the use of an elliptical body can result in a noticeably higher maximum lift-drag ratio than that obtained through use of a circular body.

2. The aerodynamic characteristics for bodies of circular and elliptic cross section and for arrow wing and body combinations can be computed reasonably well by the methods outlined in the report.

3. From this investigation it is estimated that increase of body volume by as much as 40 percent by extensions to the length results in only a small loss in maximum lift-drag ratio.

4. For fixed length, maximum lift-drag ratio decreases almost linearly with increase in body diameter.

Ames Research Center
National Aeronautics and Space Administration
Moffett Field, Calif., Jan. 27, 1959

APPENDIX

METHODS FOR COMPUTING AERODYNAMIC CHARACTERISTICS FOR BODIES AND ARROW WING AND BODY COMBINATIONS

Bodies With Circular and Elliptic Cross Sections

For slender bodies with circular and elliptic cross sections the lift, drag, and pitching-moment coefficients can be computed by the methods of references 5 and 7. Allen in reference 7 proposes a theory for predicting the forces and moments for slender bodies of revolution inclined to angles of attack considerably higher than those for which theories based only on potential flow concepts are known to apply. In this theory a crossflow lift attributed to separation is added to the lift predicted by potential theory. The viscous crossflow is considered to be independent of the axial flow and to be that of the steady flow past a circular cylinder. Although this theory is semiempirical in that experimental crossflow drag coefficients for circular cylinders are used, it has provided considerable improvement over potential theory for computing forces and moments for bodies which have cylindrical aftersections of constant diameter. For bodies of revolution the equations for lift coefficient and pitching-moment coefficient (based on wing values, A_W and $\bar{c}$) are

$$C_{L_B} = 2 \frac{A_b}{A_W} \alpha + C_{d_c} \frac{A_p}{A_W} \alpha^2 \tag{1}$$

and

$$C_{m_B} = 2 \left[\frac{Q - A_b(l - x_m)}{A_W \bar{c}} \right] \alpha + C_{d_c} \frac{A_p}{A_W} \left(\frac{x_m - x_c}{\bar{c}} \right) \alpha^2 \tag{2}$$

In equations (1) and (2) the potential components are given by the first term and the viscous by the second. The section drag coefficient for a circular cylinder placed normal to an air stream is C_{d_c}. Values of C_{d_c}, which vary with $M_\infty \sin \alpha$ and R sin α, can be obtained in reference 8. As shown in reference 5, drag coefficients for inclined bodies can be closely estimated by means of the relation

$$C_{D_B} = (C_{D_o})_B + C_{L_B} \alpha \tag{3}$$

In reference 5 it is shown that the lift and pitching-moment coefficients for a body of elliptic cross section can be correlated with the corresponding coefficients for a body of revolution having the same axial distribution of cross-sectional area. Ratios of lift coefficients and ratios of pitching-moment coefficients are given by

$$\frac{(C_{L_B})_e}{C_{L_B}} = \frac{(C_{m_B})_e}{C_{m_B}} = \frac{a}{b}\cos^2\varphi + \frac{b}{a}\sin^2\varphi \qquad (4)$$

where φ is the angle of bank about the longitudinal axis, being equal to 0° with the semimajor axis, a, horizontal, and 90° with the semiminor axis, b, horizontal. For bodies with elliptic cross sections, the lift and pitching-moment coefficients can be computed by means of equations (1), (2), and (4). The drag coefficients can be computed by use of equation (3) with elliptic body coefficients substituted for circular.

The zero-lift drag coefficient $(C_{D_o})_B$ in equation (3) is taken as the sum of the pressure drag and skin-friction drag coefficients. For minimum-drag bodies, such as the circular body considered in this investigation, pressure-drag coefficients can be determined by use of reference 9. For turbulent boundary-layer flow, the skin-friction drag coefficients can be computed by the T' method of Rubesin and Johnson as presented in reference 10. For laminar flow the Blasius equation (ref. 11) is usually satisfactory. The zero-lift drag coefficients for the elliptic bodies are assumed to be equal to those computed for equivalent bodies of revolution. This assumption is closely substantiated by the experimental results of reference 5.

Arrow Wing and Body Combinations

To compute accurately the lift, drag, and pitching-moment coefficients for an arrow wing and body combination, estimates must be made of the interference between the wing and the body. Because of mathematical complexity, most interference methods are restricted to configurations employing bodies of revolution with wings which do not have sweptback trailing edges. For an arrow wing and body combination it can be seen that the primary effects of interference can be accounted for by the assumption of a delta wing, as shown in the sketch, in place of the

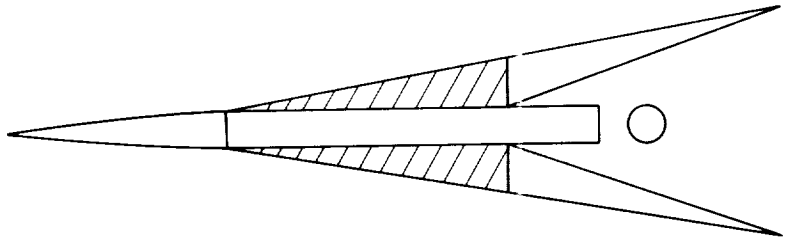

arrow wing. This assumption also permits the use of available interference factors, such as those presented in reference 12. The delta wing has the same leading-edge sweep as the arrow wing, and the trailing edge is at the rear intersection of the arrow wing with the body. The interference terminology used in this report is similar to that found in reference 12, and hence there is no detailed explanation of theory in this presentation. Force and moment equations are written for the circular body with the arrow wing. It is assumed that these expressions also can be applied to estimate the forces and moments for the elliptic body with the arrow wing.

The lift coefficient for the arrow wing and body combination is written as

$$C_L = C_{L_B} + C_{L_W} + C_{L_i} \tag{5}$$

or

$$C_L = C_{L_B} + (C_L)_{W(B)} + (C_L)_{B(W)}$$

where

$$C_{L_i} = \left\{[K_{W(B)}-1] + K_{B(W)}\right\} C_{L_W}' \frac{A_W'}{A_W} \tag{6}$$

$$(C_L)_{W(B)} = C_{L_W} + [K_{W(B)}-1] C_{L_W}' \frac{A_W'}{A_W} \tag{7}$$

and

$$(C_L)_{B(W)} = K_{B(W)} C_{L_W}' \frac{A_W'}{A_W} \tag{8}$$

In these equations C_{L_W}' and A_W' denote lift coefficient and area for the delta wing. Values of C_{L_W}', computed by linearized wing theory, can be obtained by use of reference 13. Body lift coefficients (C_{L_B}) can be computed by the method previously outlined. For the arrow-wing lift coefficients (C_{L_W}), experimental values probably should be used, since agreement of theory with experiment for efficient arrow wings has been found to be poor (ref. 3). Values for the interference factors, $K_{W(B)}$ and $K_{B(W)}$, can be obtained from the plots in reference 12 for the appropriate ratio of semispan to body radius for the delta-wing and body combination.

The drag coefficient for the complete configuration is given by

$$C_D = C_{D_W} + C_{D_B} + C_{D_i} \tag{9}$$

where

$$C_{D_i} = C_{L_i}\alpha$$

In this equation values of C_{D_B} for the body can be computed as previously outlined, but experimental values of C_{D_W} for the arrow wing probably should be used.

In the computation of center of pressure, lift coefficients can be substituted for normal-force coefficients, since they are practically equal throughout the angle-of-attack range of this investigation. The following equations are used to compute the center of pressure:

$$\bar{x} = \frac{\bar{x}_B C_{L_B} + \bar{x}_{W(B)}(C_L)_{W(B)} + \bar{x}_{B(W)}(C_L)_{B(W)}}{C_L} \tag{10}$$

where

$$\bar{x}_{W(B)} = l_N + c\left(\frac{\bar{l}}{c}\right)_{W(B)} \tag{11}$$

$$\bar{x}_{B(W)} = l_N + c\left(\frac{\bar{l}}{c}\right)_{B(W)} \tag{12}$$

$$\left(\frac{\bar{l}}{c}\right)_{W(B)} = \frac{(\bar{l}_W/c)C_{L_W} + (\bar{l}_i/c)[(C_L)_{W(B)} - C_{L_W}]}{(C_L)_{W(B)}} \tag{13}$$

$$\left.\begin{aligned} \frac{\bar{l}_i}{c}\left[(C_L)_{W(B)} - C_{L_W}\right] &= \left(\frac{\bar{l}}{c}\right)'_{W(B)}\left[C_{L_W}'\left(\frac{A_W'}{A_W}\right) + (C_L)_{W(B)} - C_{L_W}\right] - \left(\frac{\bar{l}_W}{c}\right)'\left(\frac{A_W'}{A_W}\right)C_{L_W}' \\ \text{from} \quad \left(\frac{\bar{l}}{c}\right)'_{W(B)} &= \frac{(\bar{l}_W/c)'(A_W'/A_W)C_{L_W}' + (\bar{l}_i/c)[(C_L)_{W(B)} - C_{L_W}]}{C_{L_W}'(A_W'/A_W) + (C_l)_{W(B)} - C_{L_W}} \end{aligned}\right\} \tag{14}$$

and

$$\left(\frac{\bar{l}}{c}\right)_{B(W)} = \left(\frac{\bar{l}}{c}\right)'_{B(W)} \tag{15}$$

In equations (14) and (15) the primes are used to denote quantities for the assumed delta wing. Values for $(\bar{l}/c)'_{W(B)}$ can be obtained from chart 13 in reference 12. Values for $(\bar{l}/c)'_{B(W)}$ can be obtained from chart 15 in the same reference, and $(\bar{l}_W/c)'$ is taken equal to 0.667. Computed body-alone values for $\bar{x}_B$ and experimental wing-alone values for $(\bar{l}_W/c)$ can be used.

Pitching-moment coefficients referenced to any axial length position, x_m, can be obtained by

$$C_m = (x_m - \bar{x}) \frac{C_L}{\bar{c}} \tag{16}$$

REFERENCES

1. Brown, Clinton E., and McLean, Francis E.: The Problem of Obtaining High Lift-Drag Ratios at Supersonic Speeds. I.A.S. Preprint No. 844, 1958.

2. Jones, Robert T.: Aerodynamic Design for Supersonic Speeds. Paper presented at First International Congress of the Aeronautical Sciences, Madrid, Spain, Sept. 8-13, 1958.

3. Katzen, Elliott D.: Idealized Wings and Wing-Bodies at a Mach Number of 3. NACA TN 4361, 1958.

4. Main-Smith, J. D.: Chemical Solids as Diffusible Coating Films for Visual Indications of Boundary-Layer Transition in Air and Water. R. & M. No. 2755, British A.R.C., 1954.

5. Jorgensen, Leland H.: Inclined Bodies of Various Cross Sections at Supersonic Speeds. NASA MEMO 10-3-58A, 1958.

6. Jorgensen, Leland H.: Experimental Lift-Drag Ratios for Two Families of Wing-Body Combinations at Supersonic Speeds. NACA RM A58A08, 1958.

7. Allen, H. Julian, and Perkins, Edward W.: A Study of Effects of Viscosity on Flow Over Slender Inclined Bodies of Revolution. NACA Rep. 1048, 1951.

8. Gowen, Forrest E., and Perkins, Edward W.: Drag of Circular Cylinders for a Wide Range of Reynolds Numbers and Mach Numbers. NACA TN 2960, 1953.

9. Jorgensen, Leland H.: Correlation by the Hypersonic Similarity Rule of Pressure Distributions and Wave Drags for Minimum-Drag Nose Shapes at Zero Angle of Attack. NACA RM A53F12, 1953.

10. Sommer, Simon C., and Short, Barbara J.: Free-Flight Measurements of Turbulent-Boundary-Layer Skin Friction in the Presence of Severe Aerodynamic Heating at Mach Numbers from 2.8 to 7.0. NACA TN 3391, 1955.

11. Blasius, H.: Grenezschichten in Flüssigkeiten mit Kleiner Reibung. Zeitschrift für Mathematik und Physik, vol. 56, no. 1, 1908, pp. 1-37.

12. Pitts, William C., Nielsen, Jack N., and Kaattari, George E.: Lift and Center of Pressure of Wing-Body-Tail Combinations at Subsonic, Transonic, and Supersonic Speeds. NACA Rep. 1307, 1957.

13. Stewart, H. J.: The Lift of a Delta Wing at Supersonic Speeds. Quart. Appl. Math., vol. IV, no. 3, Oct. 1946, pp. 246-254.

TABLE I.- ORDINATES FOR ARROW WING
[All dimensions are in inches]

y = 0 x_{le} = 0			y = 0.124 x_{le} = 0.700			y = 0.247 x_{le} = 1.400			y = 0.495 x_{le} = 2.800		
x_o	z_U	z_L	x_o	z_U	z_L	x_o	z_U	z_L	x_o	z_U	z_L
0	0.082	0.082	0	0.080	0.080	0	0.070	0.070	0	0.060	0.060
.350	.149	.032	.333	.151	.030	.315	.142	.029	.280	.117	.035
.700	.180	.020	.665	.178	.017	.630	.171	.017	.560	.143	.017
1.050	.200	.012	.998	.198	.011	.945	.187	.010	.840	.161	.009
1.400	.212	.008	1.330	.209	.006	1.260	.199	.005	1.120	.171	.005
1.750	.222	.005	1.663	.215	.003	1.575	.204	.003	1.400	.179	.002
2.100	.227	.003	1.995	.218	.002	1.890	.208	.001	1.680	.182	.001
2.450	.229	.002	2.328	.219	.001	2.205	.208	.001	1.960	.183	0
2.800	.227	.002	2.660	.217	.001	2.520	.205	.001	2.240	.181	-.001
3.150	.221	.001	2.993	.210	.001	2.835	.199	.001	2.520	.176	-.001
3.500	.212	.001	3.325	.202	.001	3.150	.192	0	2.800	.169	-.001
3.850	.201	0	3.658	.192	.001	3.465	.182	0	3.080	.161	-.001
4.200	.190	0	3.990	.181	.001	3.780	.171	0	3.360	.151	-.002
4.550	.175	0	4.323	.167	0	4.095	.157	0	3.640	.139	-.003
4.900	.157	0	4.655	.150	0	4.415	.141	0	3.920	.123	-.003
5.250	.135	0	4.988	.131	.001	4.725	.123	0	4.200	.110	-.003
5.600	.112	0	5.320	.109	.003	5.040	.101	0	4.480	.102	.008
5.950	.085	0	5.653	.087	.005	5.355	.078	.001	4.760	.093	.019
6.300	.058	0	5.985	.063	.008	5.670	.046	.003	5.040	.083	.033
6.650	.029	0	6.318	.038	.010	5.985	.037	.011	5.320	.069	.044
7.000	0	0	6.650	.012	.012	6.300	.025	.025	5.600	.056	.056
Leading-edge radius ≈ 0.018			0.017			0.016			0.014		

y = 0.989 x_{le} = 5.600			y = 1.484 x_{le} = 8.400			y = 1.979 x_{le} = 11.200		
x_o	z_U	z_L	x_o	z_U	z_L	x_o	z_U	z_L
0	0.050	0.050	0	0.094	0.094	0	0.285	0.285
.210	.082	.033	.140	.124	.080	.070	.292	.286
.420	.099	.009	.280	.141	.082			
.630	.113	.003	.420	.157	.087	.210	.333	.299
.840	.121	0	.560	.171	.093			
1.050	.127	-.003	.700	.184	.099	.350	.351	.311
1.260	.133	-.003	.840	.195	.107			
1.470	.140	.003	.980	.206	.116	.490	.366	.314
1.680	.147	.012	1.120	.214	.125			
1.890	.152	.021	1.260	.223	.135	.630	.379	.335
2.100	.156	.029	1.400	.229	.145			
2.310	.158	.038	1.540	.236	.156	.770	.388	.349
2.520	.159	.047	1.680	.242	.167			
2.730	.159	.056	1.820	.248	.179	.910	.395	.362
2.940	.157	.066	1.960	.254	.191			
3.150	.155	.075	2.100	.258	.205	1.050	.399	.375
3.360	.151	.087	2.240	.261	.218			
3.570	.147	.098	2.380	.264	.230	1.190	.402	.387
3.780	.143	.111	2.520	.265	.244			
3.990	.139	.124	2.660	.267	.257	1.330	.405	.399
4.200	.137	.137	2.800	.269	.269	1.400	.406	.406
Leading-edge radius ≈ 0.011			0.007			0.003		

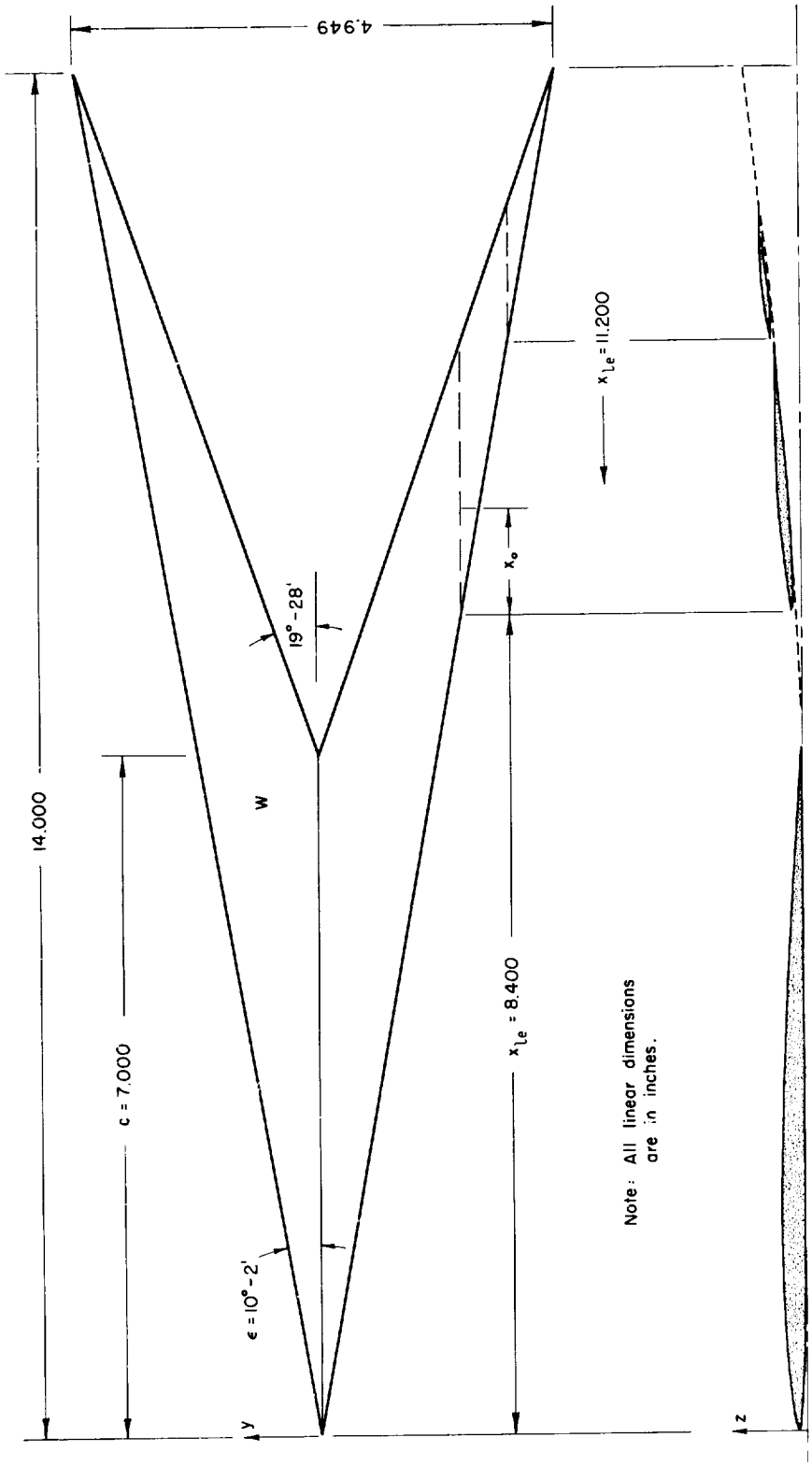

(a) Plan-form view and typical airfoil sections of wing W.

Figure 1.- Models tested.

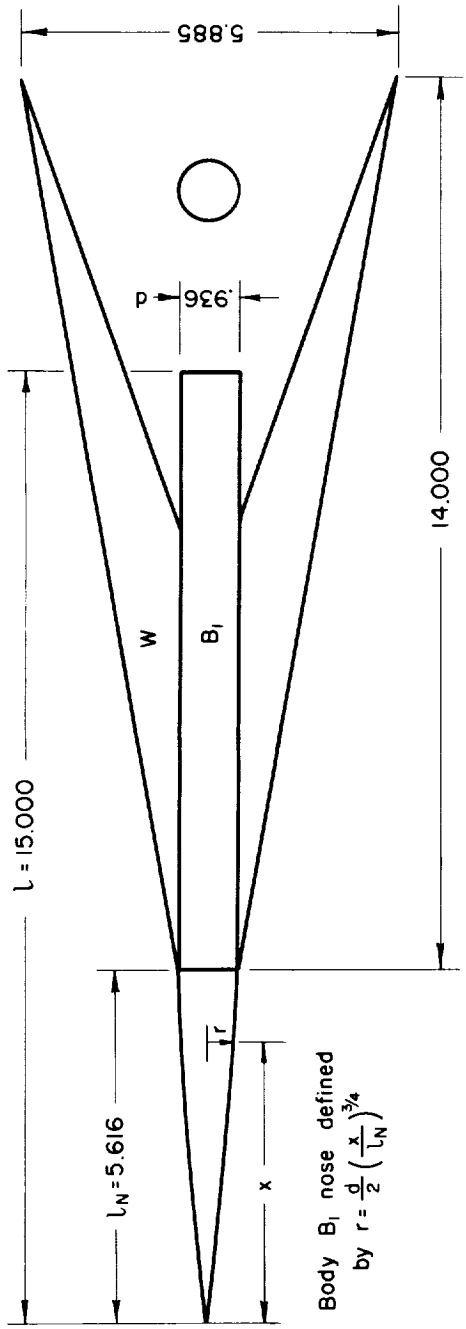

(b) Plan-form view of circular body B_1 with wing W.

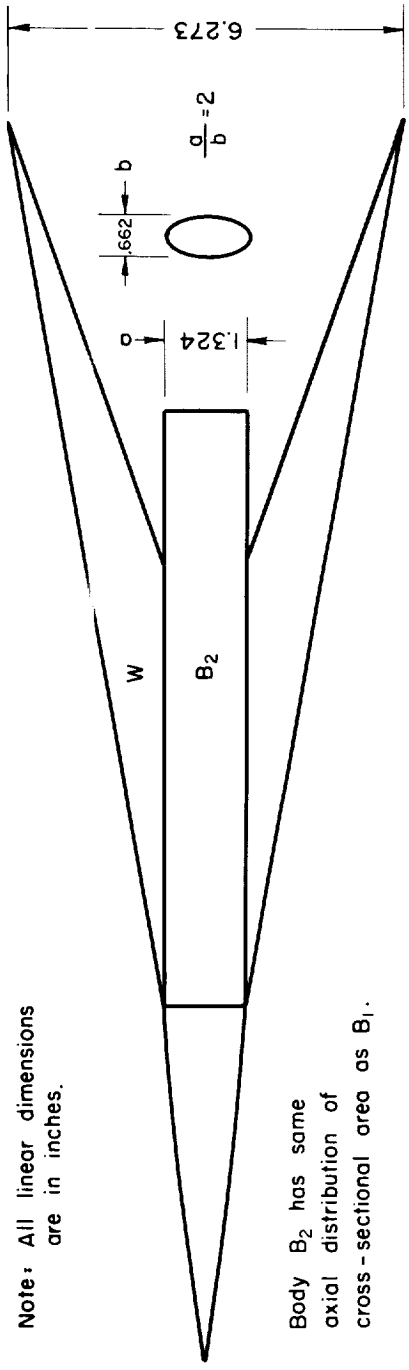

Note: All linear dimensions are in inches.

(c) Plan-form view of elliptic body B_2 with wing W.

Figure 1.- Concluded.

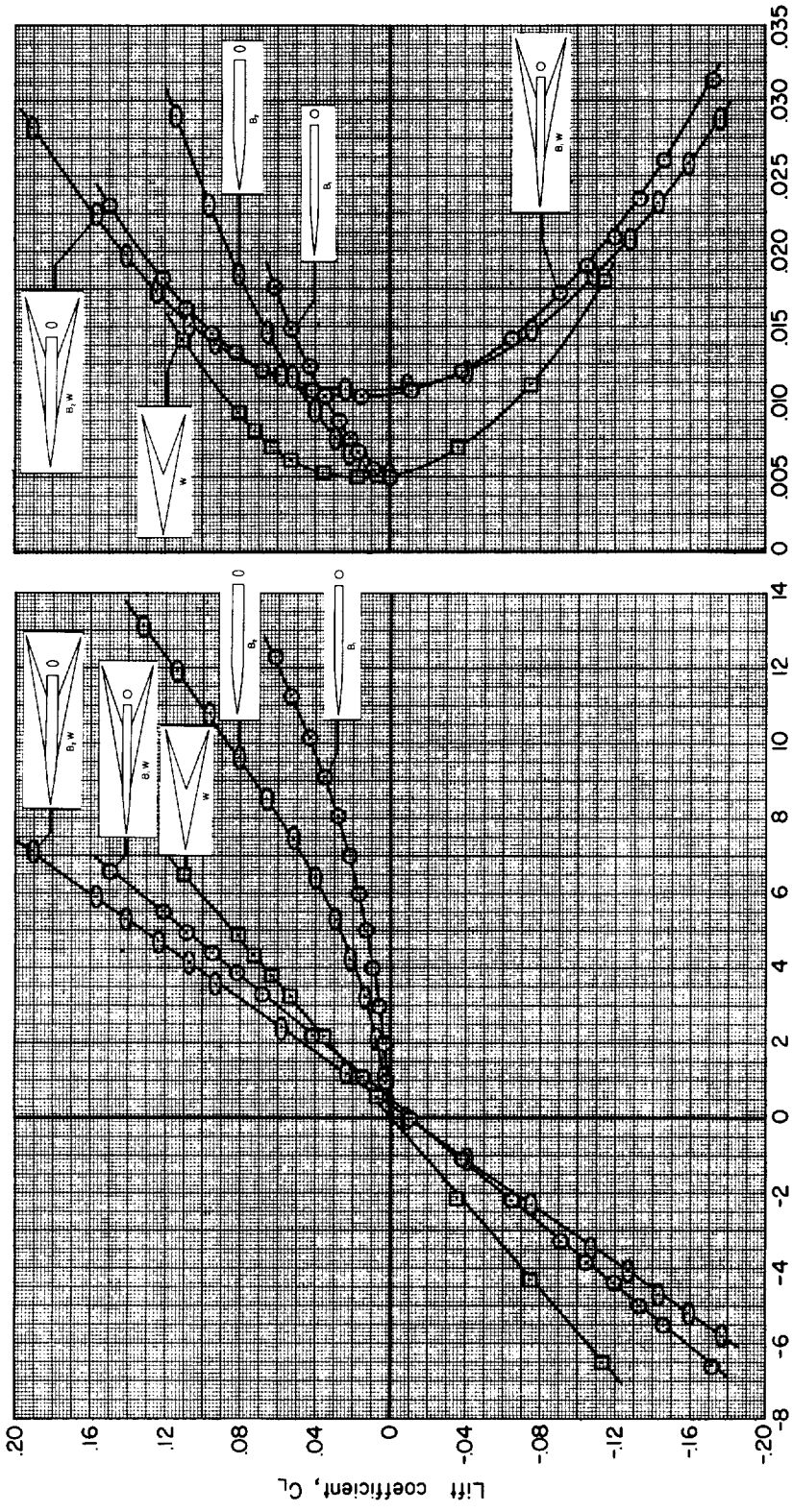

(a) Lift.

(b) Lift-drag polar.

Figure 2.- Experimental aerodynamic characteristics of models tested; $M_\infty = 2.94$, $R = 3.5 \times 10^6$.

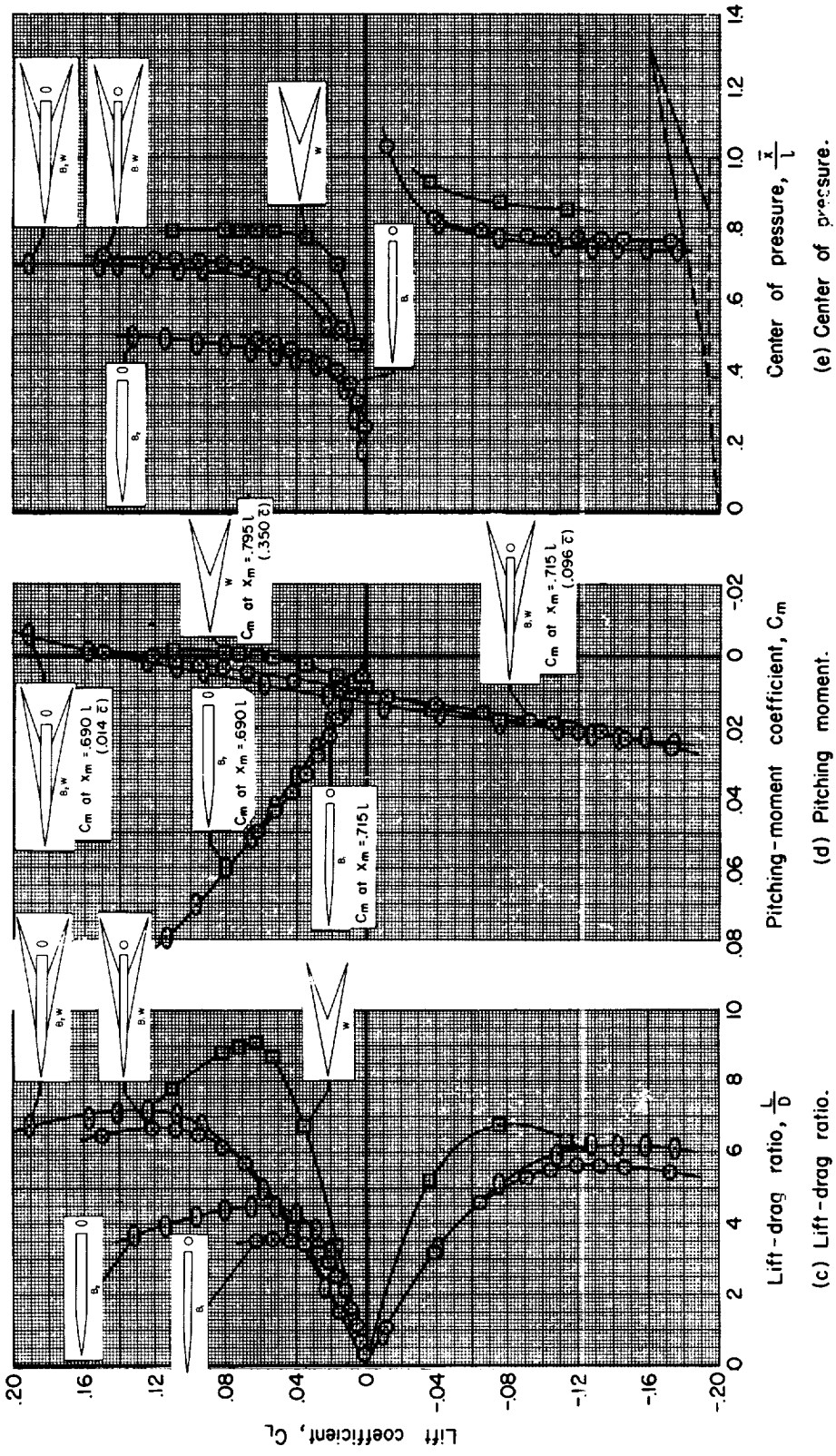

Figure 2.- Concluded.

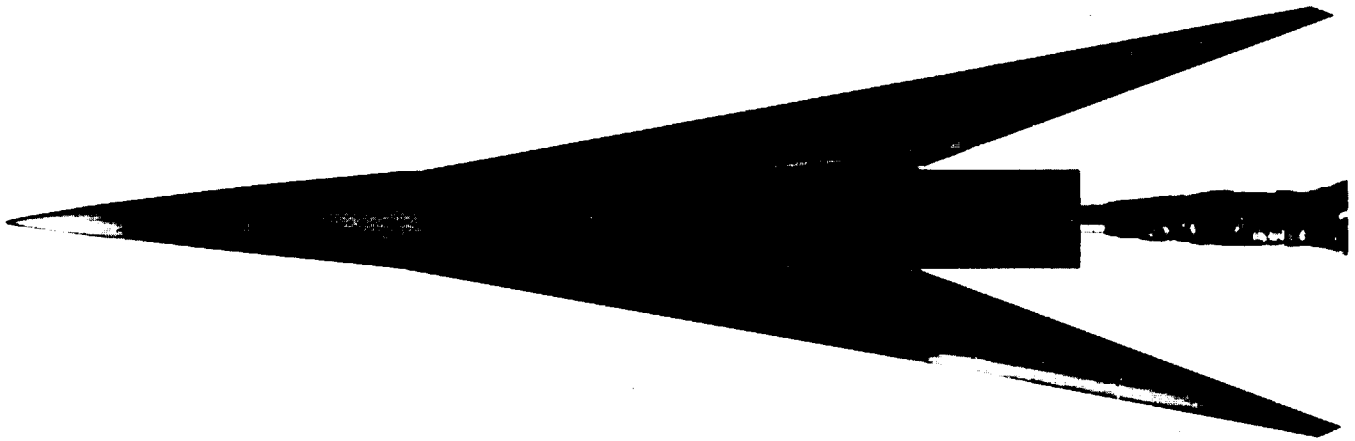

Top

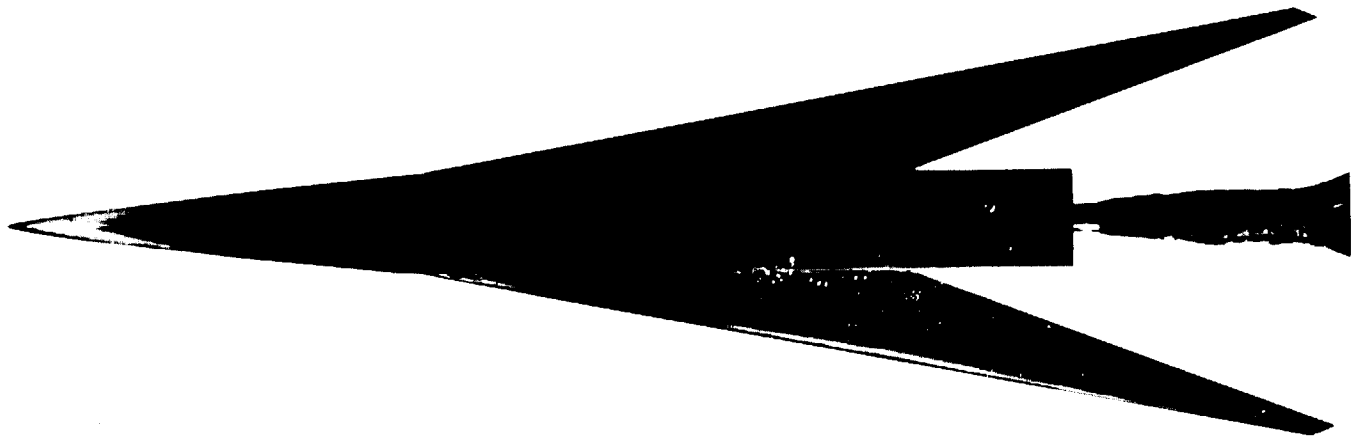

Bottom

Figure 3.- Flow patterns resulting from sublimation tests of model B_2W at $\alpha = 0^\circ$; $M_\infty = 2.94$, $R = 3.5 \times 10^6$.

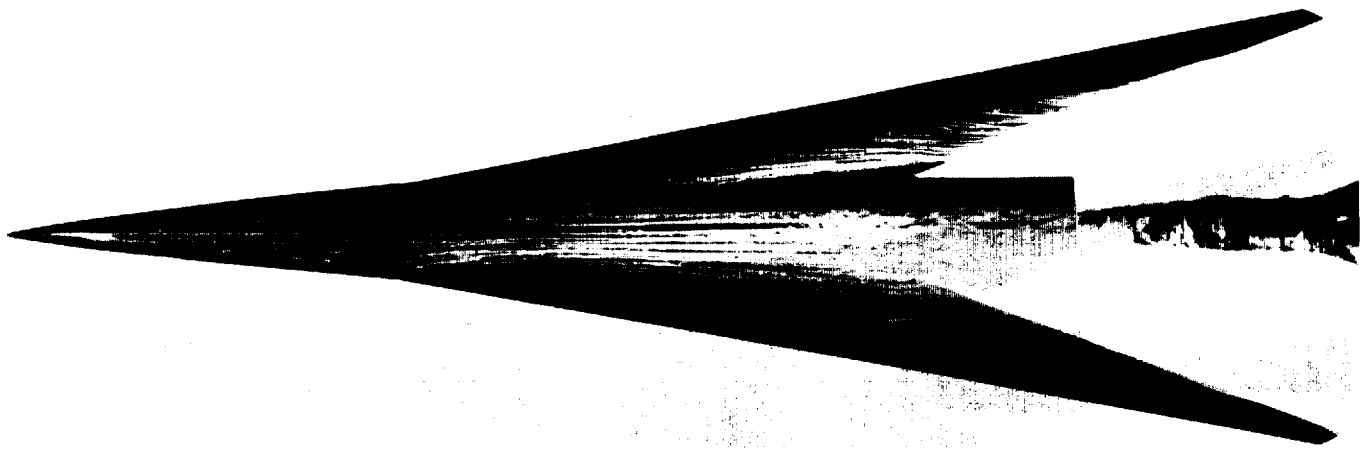

Top

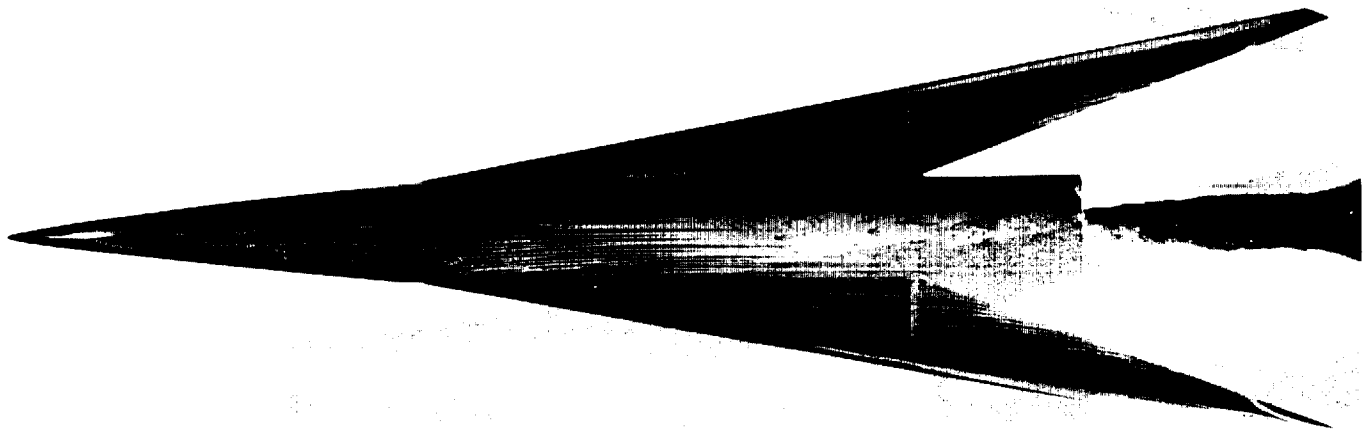

Bottom

(a) $\alpha = 0^{o}$

Figure 4.- Flow patterns resulting from white-lead tests of model B_2W; $M_\infty = 2.94$, $R = 3.5 \times 10^6$.

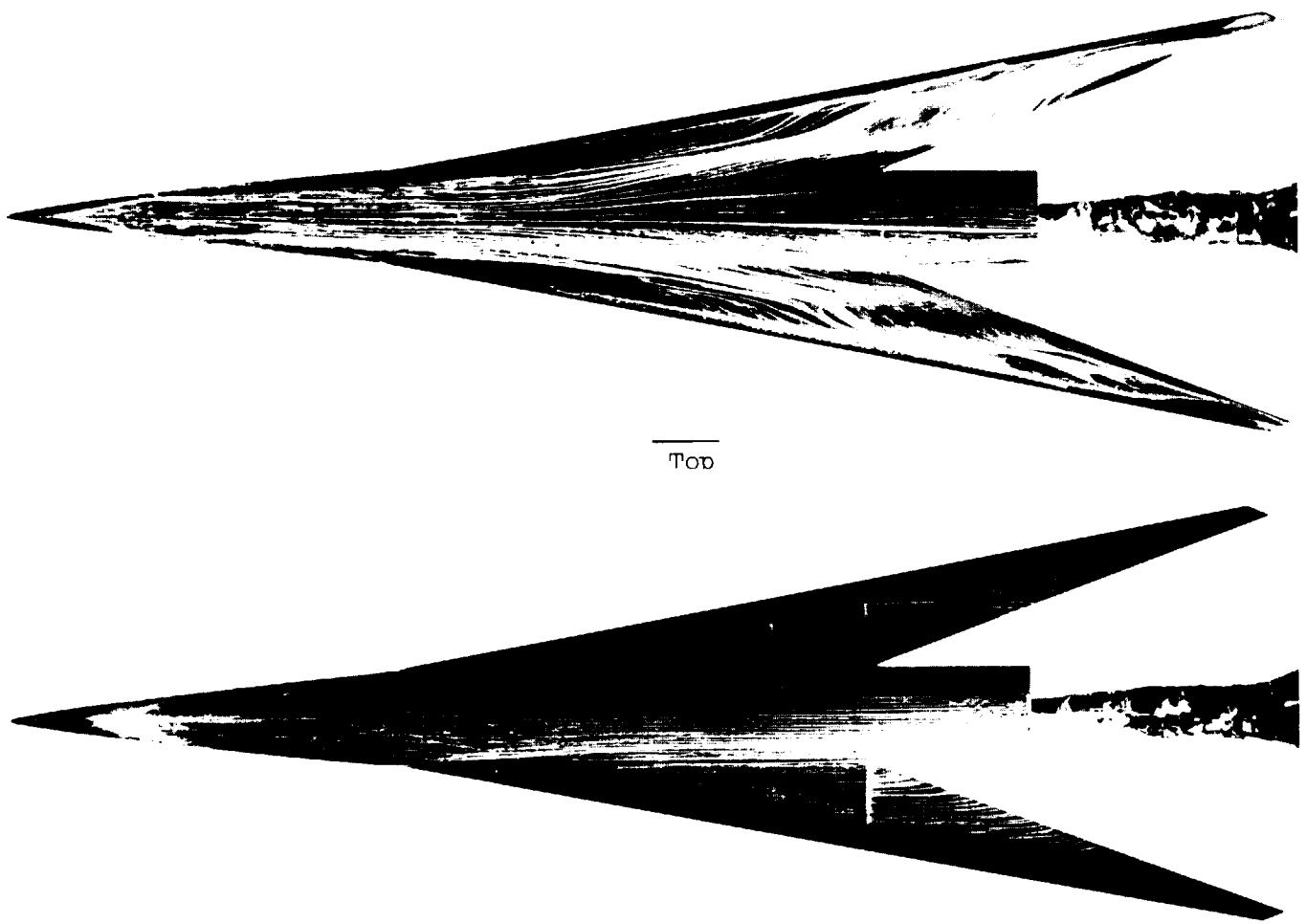

Top

Bottom

(b) $\alpha = 4.5^{\circ}$

Figure 4.- Concluded.

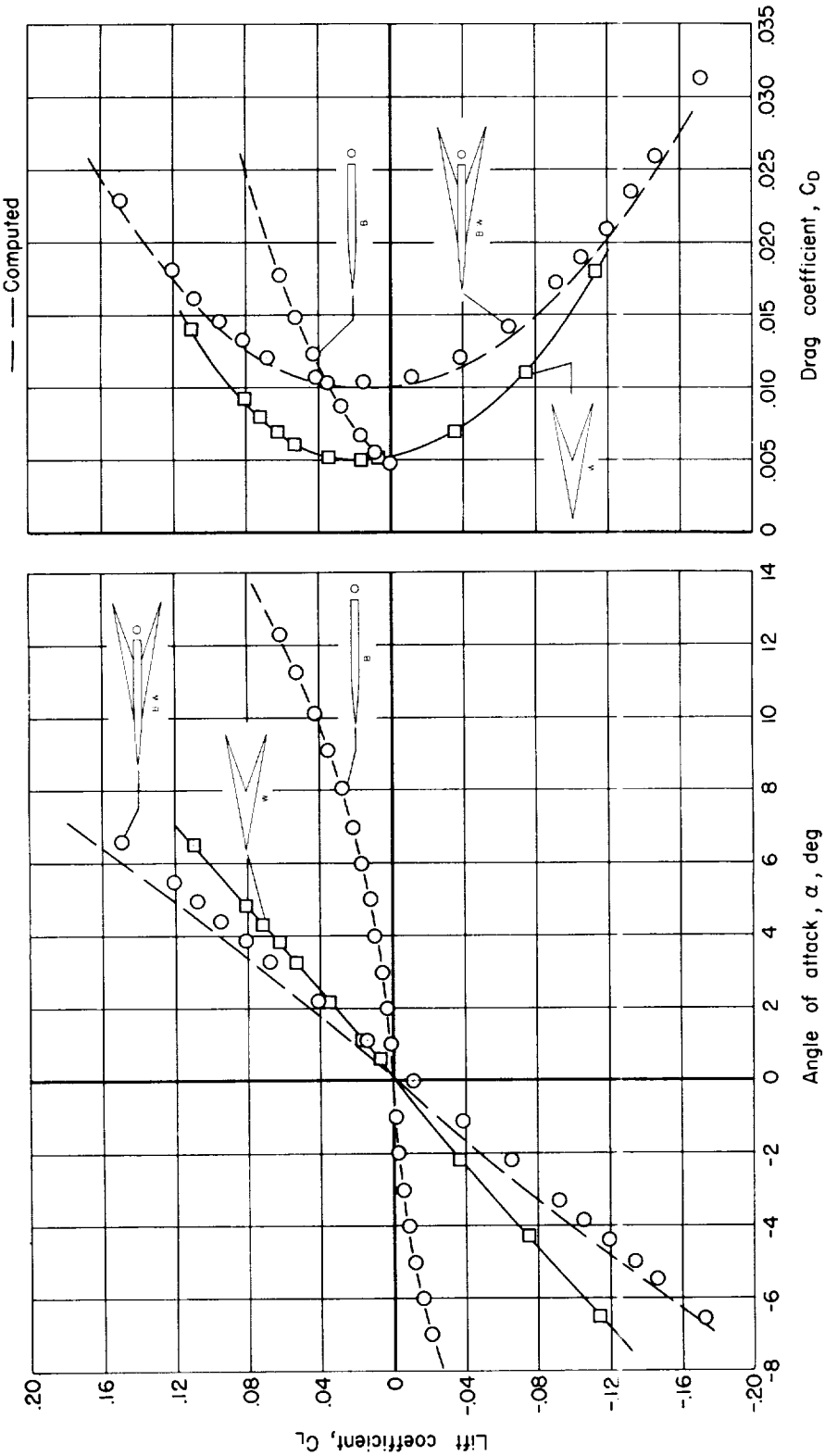

Figure 5.- Comparisons of predicted and experimental aerodynamic characteristics for circular body B_1 and wing-body combination B_1W; $M_\infty = 2.94$, $R = 3.5 \times 10^6$.

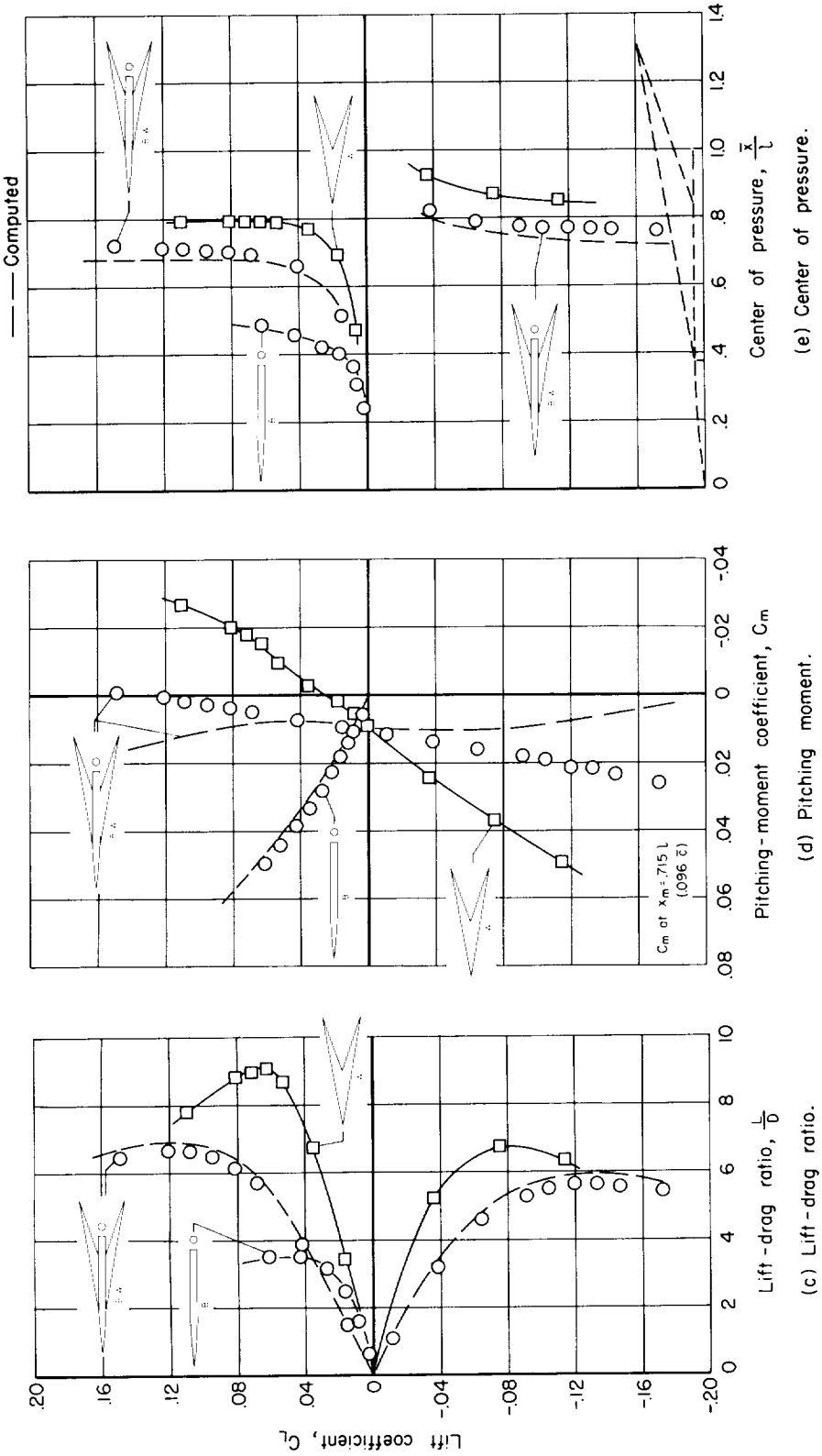

Figure 5.- Concluded.

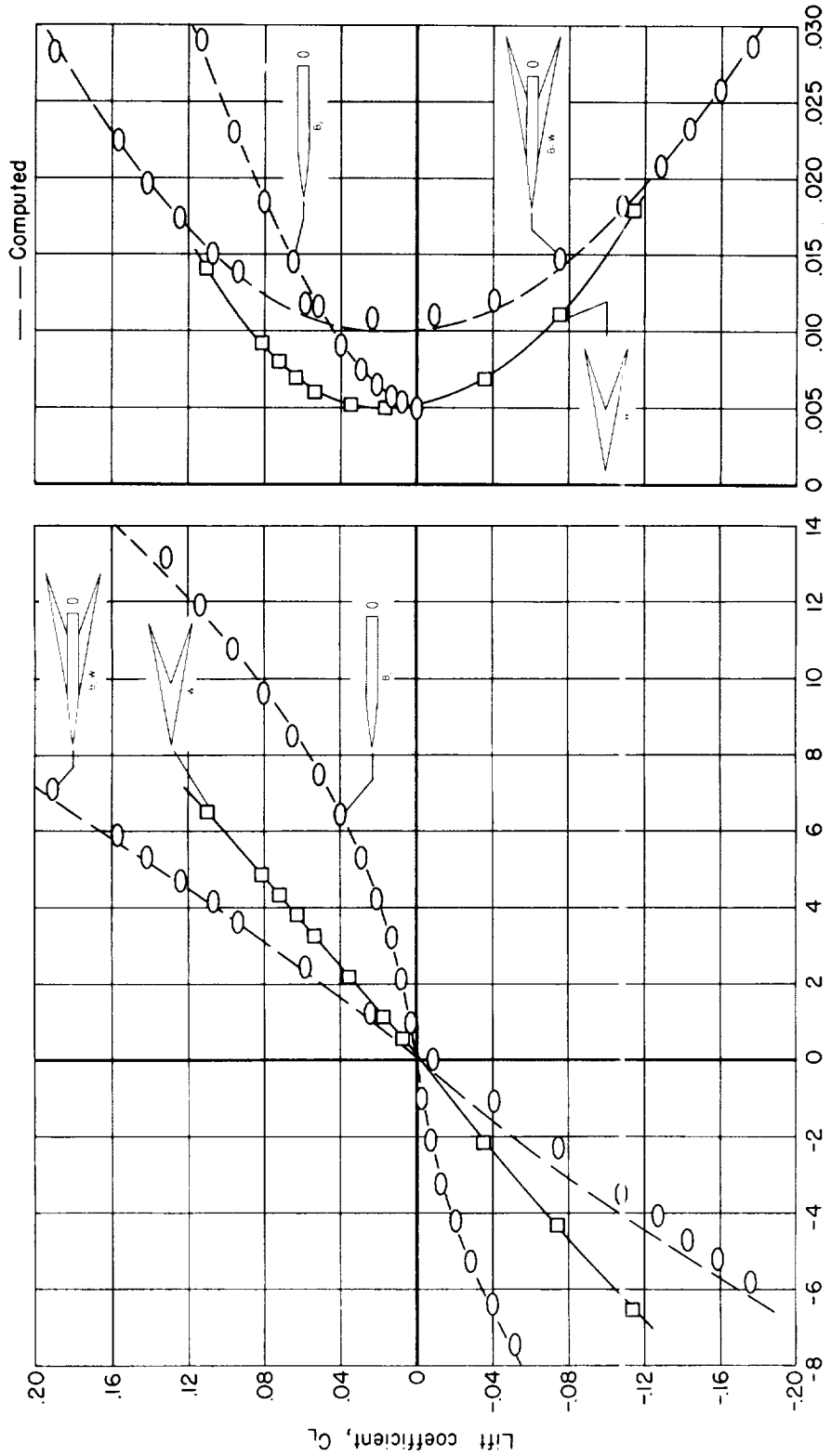

(a) Lift.

(b) Lift-drag polar.

Figure 6.- Comparisons of predicted and experimental aerodynamic characteristics for elliptic body B_2 (a/b = 2) and wing-body combination B_2W; M_∞ = 2.94, R = 3.5×10^6.

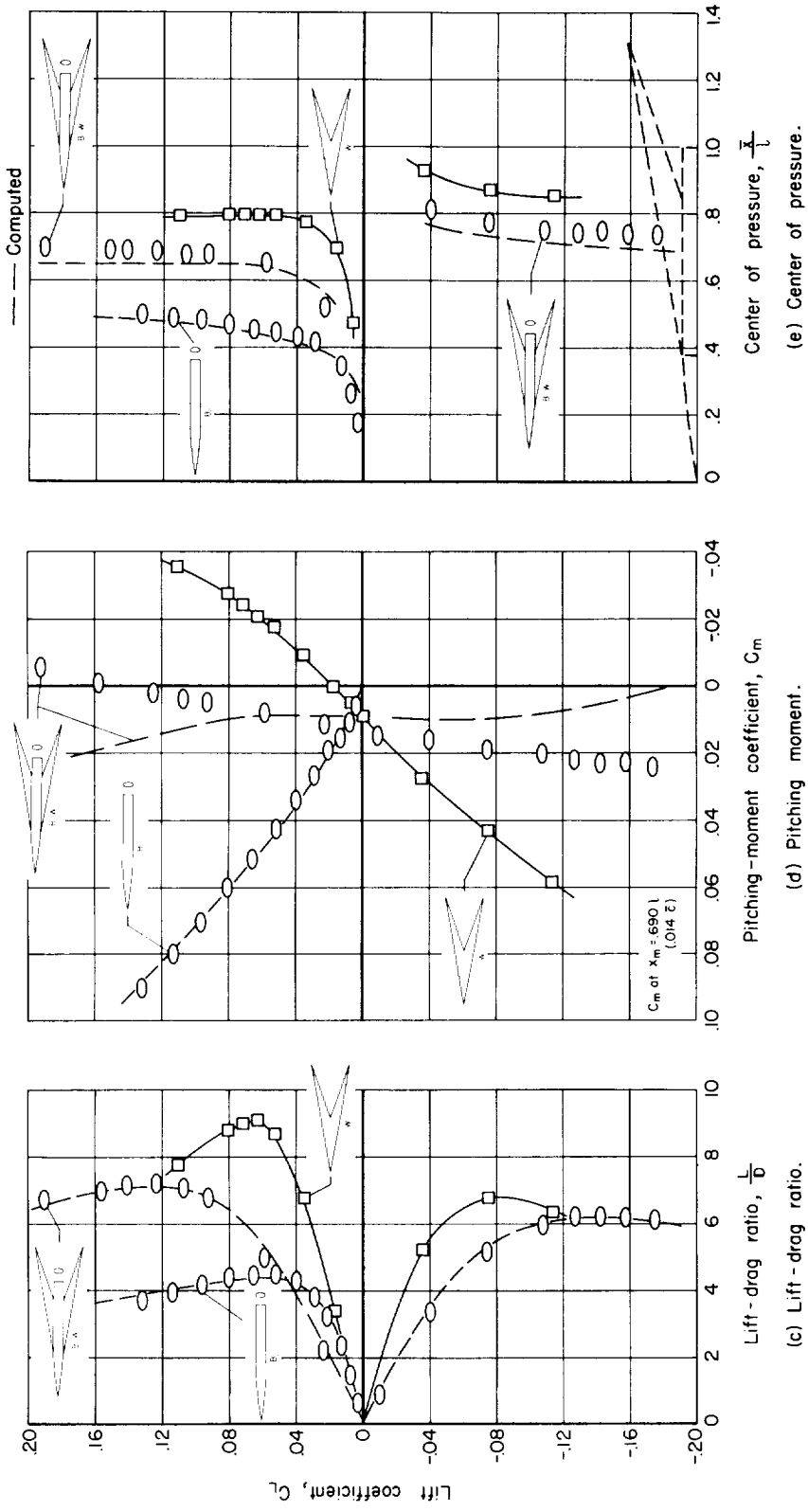

Figure 6.- Concluded.

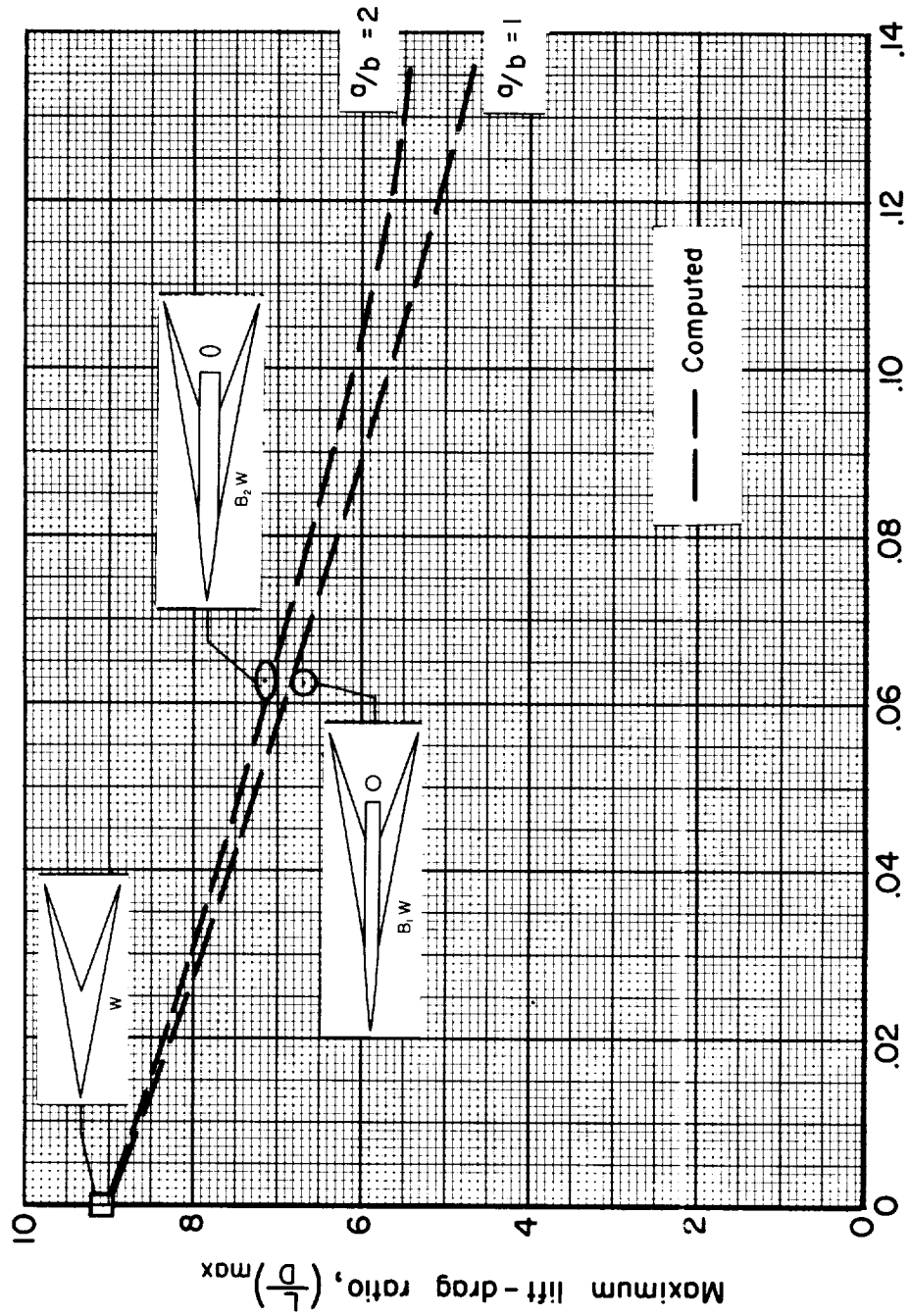

Figure 7.- Effect of body diameter on maximum lift-drag ratio for wing-body combinations with body and wing lengths fixed; $l/c = 2.143$, $l/l_N = 2.667$, $M_\infty = 2.94$, $R = 3.5 \times 10^6$.

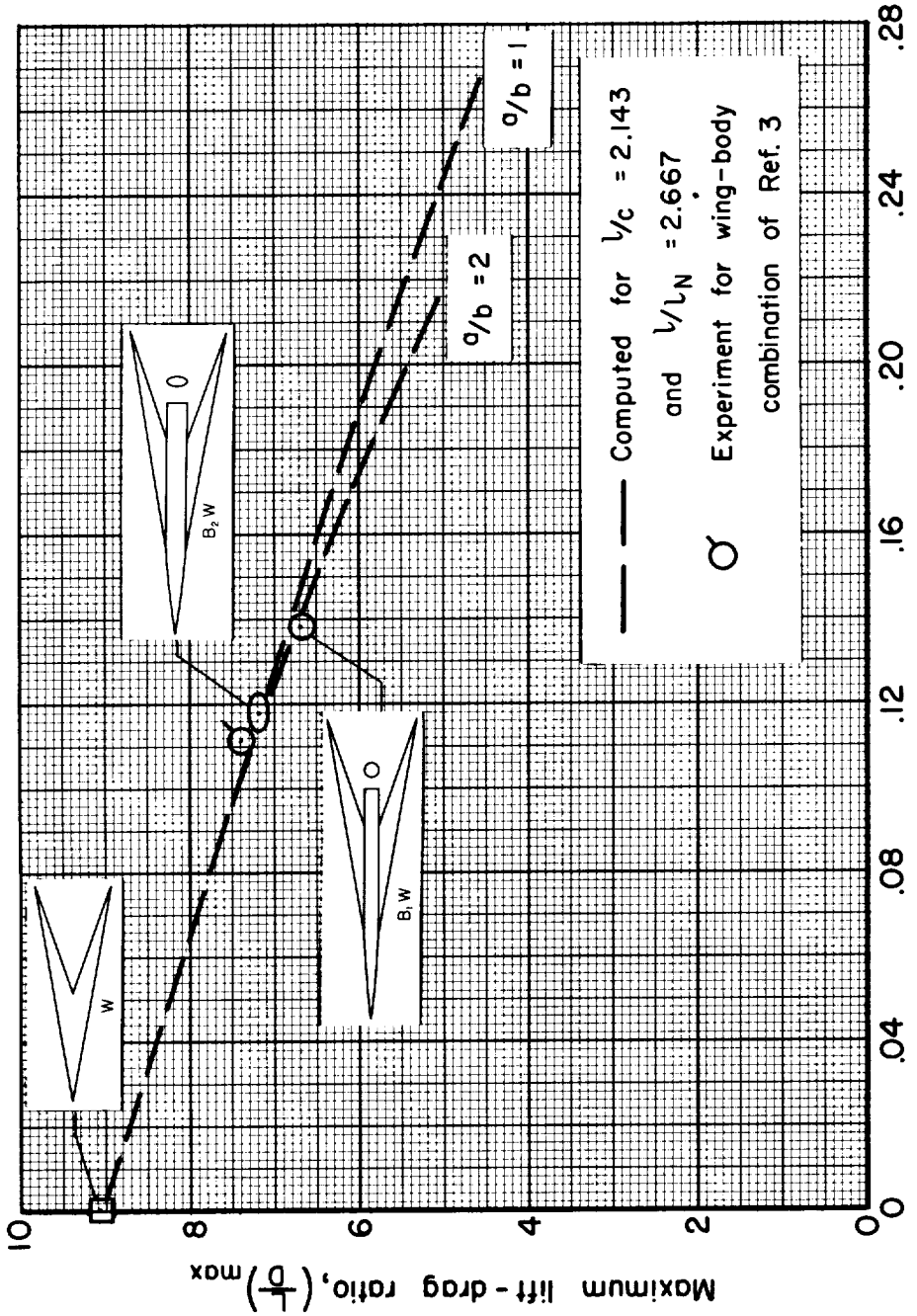

Figure 8.- Effect of body volume on maximum lift-drag ratio for wing-body combinations; M_∞ = 2.94, R = 3.5×10^6.

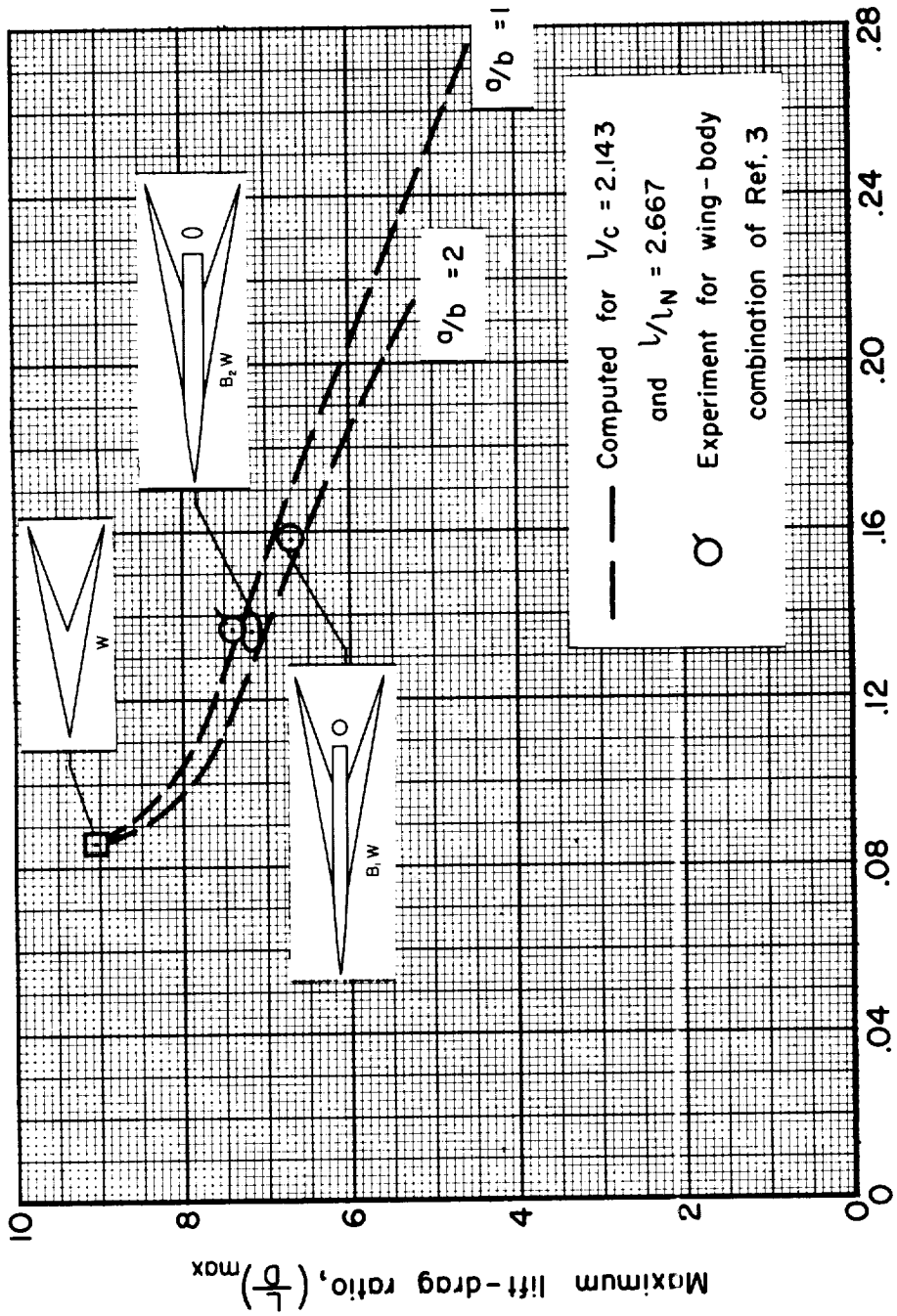

Figure 9.- Effect of total volume on maximum lift-drag ratio for wing-body combinations; $M_\infty = 2.94$, $R = 3.5 \times 10^6$.